ACS APPLIED BIO MATERIALS

www.acsabm.org Article

Tunable Drug Release through Varying Drug Affinities for Ocular Chronic Disease

Hyeonah Lee, Serim Byun, Moonyoung Kim, Hyeokjung Kim, and Hyeran Noh*

Cite This: https://doi.org/10.1021/acsabm.5c00425 Read Online

ACCESS | Metrics & More | Article Recommendations | Supporting Information

ABSTRACT: Effective drug delivery is critical for the management of chronic diseases such as glaucoma, where sustained therapeutic levels can significantly enhance treatment outcomes. In this study, we present a Particles-on-a-Gel (PoG) system that leverages differential nanocarrier affinities to modulate drug release kinetics. By integrating poly(N-isopropylacrylamide) nanogels (pNIPAM) and silver nanoparticles (AgNPs), the PoG platform enables both controlled initial release and prolonged drug delivery. Isothermal titration calorimetry (ITC) was employed to quantitatively characterize the thermodynamic interactions between timolol maleate and the nanocarriers, revealing distinct binding modalities—hydrophobic interactions with pNIPAM and chemically driven binding with AgNPs. These findings underscore the role of thermodynamic tuning in optimizing drug-carrier interactions to enhance release profiles and retention. Furthermore, incorporation of the PoG system into a contact lens-based drug delivery platform demonstrated its translational potential, maintaining optical transparency while enabling sustained drug release. Overall, this work highlights the promise of thermodynamically guided nanocarrier design in developing patient-centric drug delivery systems for chronic disease management.

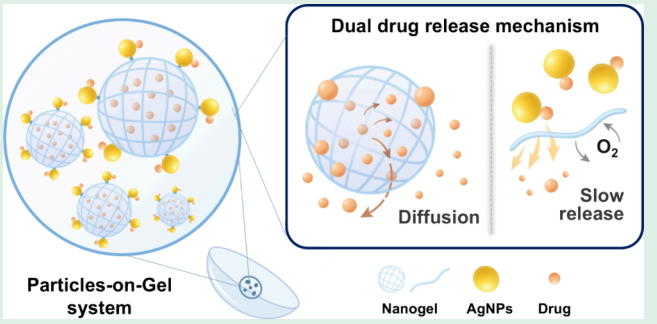

KEYWORDS: *sustained drug release, dual-nanocarrier system, thermodynamic drug binding, tunable release kinetics, ocular drug delivery*

1. INTRODUCTION

Chronic diseases, such as glaucoma, pose significant health risks, particularly among the elderly. Effective management of these conditions remains a challenge due to the need for consistent and long-term medication adherence. Rapid drug clearance and poor patient compliance often result in fluctuating intraocular drug concentrations, which can diminish therapeutic efficacy and increase the risk of disease progression.[1] To address these challenges, researchers have explored advanced drug delivery systems—including liposomes, nano- and microcapsules, and metal-based carriers—that improve drug solubility, protect drugs from degradation, and enable site-specific delivery.[2−6]

Despite these advancements, achieving sustained and precisely controlled drug release remains difficult, particularly in the context of chronic ocular therapy. Recent efforts have focused on active-targeted delivery, which facilitates site-specific drug release in response to external stimuli, such as temperature, light, or magnetic fields.[7−9] While these methods are promising, they may not be suitable for sensitive tissues like the eye, where such stimuli could cause adverse effects or are impractical for long-term use.[10,11] Thus, there is a critical need for alternative drug delivery strategies capable of providing prolonged, controlled release without reliance on external triggers.

In response to this need, we propose a novel drug delivery platform that utilizes carriers with differential binding affinities to enable temporally controlled drug release. By leveraging the varying strengths of drug-carrier interactions, this system facilitates a sequential, sustained release profile, extending therapeutic effects and reducing the frequency of administration. This strategy is particularly advantageous for the treatment of chronic ocular diseases, such as glaucoma, where long-term, stable drug delivery is essential.

To realize this approach, we developed the Particles-on-a-Gel (PoG) system—a composite carrier consisting of poly(N-isopropylacrylamide) nanogels (pNIPAM) and silver nanoparticles (AgNPs). In this system, pNIPAM nanogels provide a biocompatible hydrogel matrix with hydrophobic interaction sites for drug loading and structural support for nanoparticle integration. In turn, AgNPs offer strong surface binding affinity and high reactivity, enhancing drug loading and enabling the formation of a heterogeneous binding environment. While

Received: March 5, 2025
Revised: June 9, 2025
Accepted: June 10, 2025

https://doi.org/10.1021/acsabm.5c00425
ACS Appl. Bio Mater. XXXX, XXX, XXX−XXX

AgNPs may raise concerns regarding long-term biocompatibility or toxicity, the nanoparticles used in this study are embedded in a hydrogel matrix, which helps retain them in place and reduces the likelihood of direct contact with ocular tissues during application. These complementary functions allow the PoG system to achieve tunable and sustained drug release through intrinsic carrier−drug interactions, without the need for external stimuli.

In this study, we selected timolol maleate—a commonly prescribed β-blocker for glaucoma treatment—as the model drug to evaluate the PoG system. Thermodynamic interactions between the drug and carriers were quantitatively assessed using isothermal titration calorimetry (ITC), which provided insights into the distinct binding mechanisms: hydrophobic interactions with pNIPAM and chemically driven binding with AgNPs. This thermodynamic analysis was further supported by kinetic modeling to characterize the drug release dynamics and optimize delivery performance.[12−14]

To demonstrate the clinical potential of the PoG system, we incorporated it into a contact lens-based drug delivery platform, capitalizing on the lens's established utility in ocular drug administration. This integrated system allows for precise, sustained, and patient-friendly drug release without the need for external activation, maintaining optical transparency and therapeutic efficacy over extended periods.[15−17]

This study presents a thermodynamically guided drug delivery approach based on differential binding affinities, offering a promising solution for sustained ocular drug release. By combining biocompatible hydrogel matrices with functional nanomaterials such as silver nanoparticles, and integrating thermodynamic and kinetic analyses, this platform lays the groundwork for the development of adaptive, patient-specific treatments for chronic eye diseases like glaucoma.

2. EXPERIMENTAL SECTION

2.1. Materials. Ethylene Glycol (≥99. 5%) (EG) was purchased from Duksan Pure Chemicals (Korea). N,N'-Methylenebis-(acrylamide) (≥99. 5%) (BIS), Ethyl alcohol (94.5%) was purchased from Samchun Chemicals (Korea). Phosphate Buffered Sahlin (PBS) was purchased from Amresco (USA). Silver nitrate ($AgNO_3$), Polyvinylpyrrolidone (K30) (PVP), Ammonium Persulfate (≥98%) (APS), Methyl alcohol (≥99.9%) were purchased from Daejung Chemicals (Korea). *N*-Isopropylacrylamide (≥97%) (NIPAAm), Sodium Dodecyl Sulfate (≥99%) (SDS), Methacrylic acid (≥99%) (MAA), Ethylene Glycol Dimethacrylate (98%) (EGDMA), Azobis-(isobutyronitrile) (AIBN), Timolol maleate (≥98%), Dialysis tubing cellulose membrane were all purchased from Sigma-Aldrich (USA). 1-Day Acuvue Moist contact lenses were obtained from Acuvue, Johnson & Johnson.

2.2. Preparation of Individual Carrier. Silver nanoparticles (AgNPs) were synthesized via a polyol process.[18] A 30 mM solution of Ethylene Glycol (EG) and Polyvinylpyrrolidone (PVP) was heated to 120 °C in a three-neck flask. Subsequently, a 250 mM EG/silver nitrate solution was added, and the reaction mixture was maintained at this temperature for an additional 30 min.

For the synthesis of pNIPAM nanogels, *N*-Isopropylacrylamide (NIPAM), methacrylic acid (MAA), N, N'-Methylenebis(acrylamide) (BIS), and sodium dodecyl sulfate (SDS) were dissolved in distilled water and sonicated for 1 h. The resulting solution was heated to 70 °C under nitrogen gas for 30 min, followed by the addition of ammonium persulfate (APS) as an initiator. The reaction was continued under the same conditions for 4 h. After synthesis, the pNIPAM nanogels were cooled to room temperature and transferred to a dialysis membrane, then dialyzed against distilled water for 7 days with daily water changes.

The morphology of both AgNPs and pNIPAM nanogels was examined using transmission electron microscopy (TEM). Samples were drop-cast onto carbon-coated copper grids and imaged using a JEOL JEM-2010 microscope.

The chemical structure of pNIPAM was analyzed using proton nuclear magnetic resonance (1H NMR) spectroscopy (Bruker Ascend Evo, 400 MHz). Prior to measurement, freeze-dried pNIPAM was redispersed in deuterium oxide (D_2O). Furthermore, elemental composition was assessed via energy-dispersive X-ray spectroscopy (EDS), performed in conjunction with scanning electron microscopy (SEM; Tescan TESCAN VEGA3). EDS measurements were conducted on contact lenses prepared by copolymerizing (Hydroxyethyl)methacrylate (HEMA) with either pNIPAM nanogels or timolol-loaded pNIPAM nanogels. Lenses composed of HEMA only were used as controls.

2.3. Determination of Carrier-Timolol Binding Profiles. *2.3.1. Isothermal Titration Calorimetry (ITC) Analysis.* Isothermal titration calorimetry (ITC) measurements were performed using a MicroCal PEAQ-ITC instrument (Malvern Panalytical). Timolol maleate was dissolved in distilled water, while AgNPs were diluted in a 5% ethylene glycol solution. The standard titration protocol consisted of 18 successive injections of timolol maleate, administered at 180-s intervals into a sample cell containing AgNPs. The reference cell was filled with 5% ethylene glycol solution, and the sample cell was continuously stirred at 500 rpm throughout the procedure.

For the ITC analysis of pNIPAM nanogels, timolol maleate was loaded into the sample cell, while the pNIPAM nanogels suspension was placed in the syringe. Distilled water was used in the reference cell, and all other experimental conditions were kept consistent with those used in the AgNPs analysis. The order of addition of timolol maleate was reversed in this case due to experimental considerations: the syringe typically contains the higher-concentration component to allow for optimal detection of binding events. The heat of dilution from titrating timolol maleate into the buffer was measured separately and subtracted from the corresponding data sets; all data were normalized to zero prior to analysis.

Thermodynamic parameters, including binding stoichiometry (n), affinity constant (K_a), and other relevant values, were derived using the integrated Origin software (OriginLab). Reported values represent the mean values from two independent experiments.

2.3.2. Differential Scanning Calorimetry (DSC) Analysis. Differential scanning calorimetry (DSC) was performed to assess the thermal properties of the contact lens formulations. Measurements were conducted in the dry state following lens fabrication, using the preparation method described in Section 2.5. Thermal analysis was carried out using Q100 DSC from TA Instruments under a nitrogen atmosphere. Heat flow was recorded over a temperature range of 40−120 °C at a controlled heating rate.

2.4. Synthesis of Particles-on-a-Gel System. A solution of silver nanoparticles (AgNPs) and timolol maleate was prepared at a concentration of 200 μM with a 1:4 molar ratio and incubated at 40 °C for 8 h. Simultaneously, for the pNIPAM nanogels formulation, pNIPAM was mixed with timolol maleate at an equivalent molar ratio and stirred at 70 rpm at 25 °C. The Particles-on-a-Gel (PoG) system was subsequently formed by combining the preincubated pNIPAM-timolol and AgNPs-timolol complexes in a 1:1 molar ratio, followed by incubation at 25 °C with continuous agitation at 70 rpm.

For morphological analysis, the PoG solution was deposited as a thin film using a spin coater and dried overnight at room temperature. The resulting samples were then imaged using scanning electron microscopy (FIB Quanta 3D FEG, Cryo mode) to evaluate the structural integration of AgNPs within the pNIPAM matrix.

2.5. Determining Drug Release Profiles of the PoG System. The drug release behavior of the Particles-on-a-Gel (PoG) system and the individual base carriers was evaluated using a contact lens format. Prior to drug loading, commercial contact lenses were thoroughly cleaned by alternating washes with acetone and distilled water several times to remove any potential surface residues.

For drug loading, lenses were immersed overnight at room temperature in a preprepared carrier solution containing timolol

https://doi.org/10.1021/acsabm.5c00425
ACS Appl. Bio Mater. XXXX, XXX, XXX−XXX

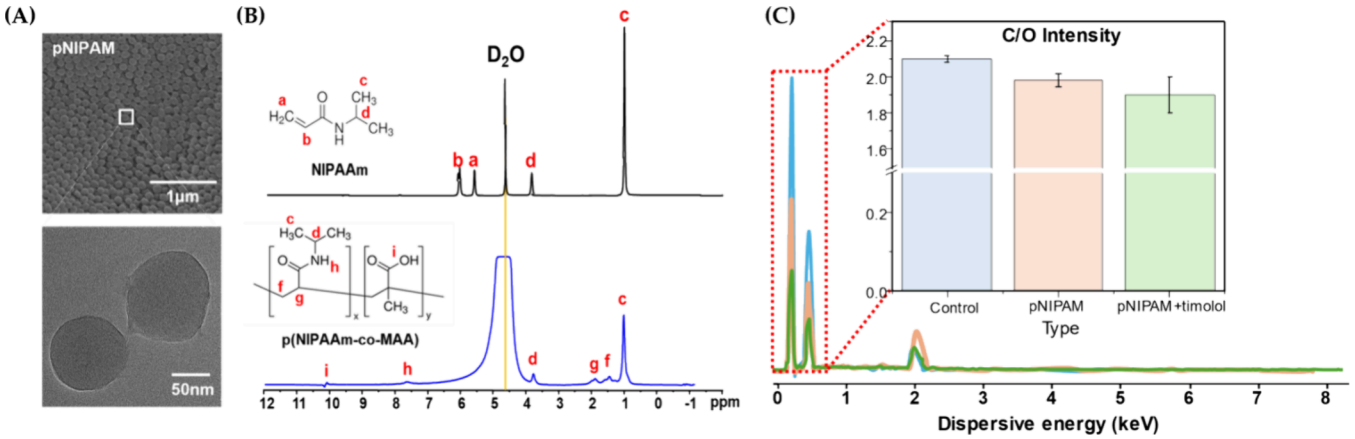

Figure 1. Morphological characterization of pNIPAM nanogels. (A) Electron microscopy image, (B) 1H NMR spectrum recorded in D_2O at 700 MHz, and (C) energy-dispersive X-ray spectroscopy (EDS) analysis measured in contact lens form. The control sample consists of a contact lens made of HEMA alone, while the pNIPAM-loaded sample refers to a HEMA-based contact lens incorporating pNIPAM. The pNIPAM-Timolol sample consists of a HEMA-based contact lens loaded with pNIPAM containing timolol maleate.

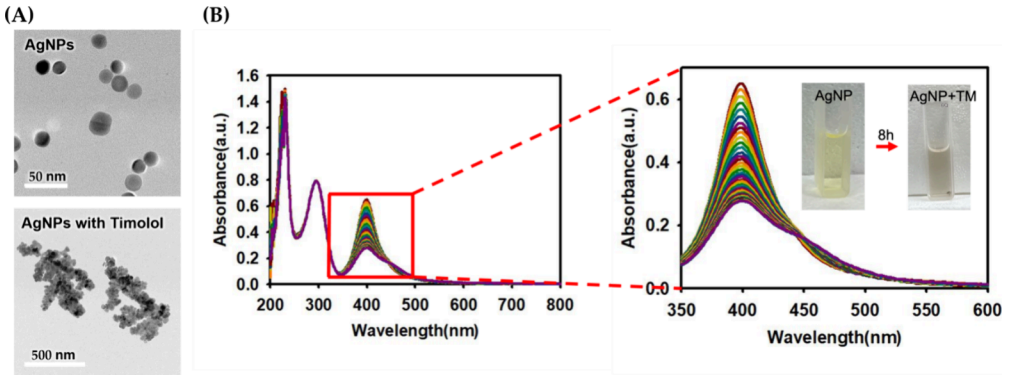

Figure 2. Characterization of AgNPs and their interaction with timolol maleate. (A) TEM images of AgNPs and AgNPs bound with timolol. (B) 8-h kinetic profile of AgNPs with timolol maleate at 25 °C.

maleate. The PoG carrier solution was prepared by combining AgNP-timolol and pNIPAM-timolol complexes, each preincubated as described in Section 2.4, in a 1:1 molar ratio. The final concentration of timolol maleate in the solution was adjusted to 200 μM. This incubation step allowed for diffusion-driven absorption of drug-loaded carriers into the hydrogel matrix of the contact lenses. After incubation, unbound drug and excess carriers were removed by rinsing the lenses with distilled water, ensuring that only drug-loaded lenses were used for subsequent analysis.

To evaluate the release profiles, each lens was placed in 400 μL of artificial tear fluid and incubated at 32 °C to simulate physiological ocular conditions. The cumulative release of timolol maleate was monitored over time using UV−visible spectroscopy. To improve measurement accuracy, an additional sample preparation step was performed before analysis: hydrochloric acid (HCl) was added to the release medium, followed by centrifugation to precipitate interfering ions. This step minimized background absorbance and enhanced the specificity of the assay. The concentration of released timolol maleate was quantified based on its characteristic absorbance peak at 295 nm, corresponding to the free drug dissociated from the nanocarriers.

The artificial tear fluid was prepared with the following composition: distilled water (3 L), NaCl (15.252 g), KCl (4.248 g), sodium citrate (1.338 g), glucose (0.108 g), $CaCl_2$ (1.662 g), urea (0.216 g), sodium carbonate (3.816 g), HCl (2.844 mL), egg albumin (11.4 g), and human IgG (0.0276 g), adjusted to pH 7.0. All experiments were performed in triplicate, with 400 μL of artificial tear fluid used per sample.

2.6. Kinetic Analysis of Drug Release. Drug transport constants (k_1, k_2) and transport exponents (n, m) for the different formulations were determined by fitting the in vitro drug release data to the Korsmeyer-Peppas and Peppas-Sahlin models using the DDSolver program (China Pharmaceutical University, Nanjing, China). Microsoft Office Excel (Microsoft Corporation, Redmond, USA), integrated as a module within DDSolver, was used to perform the nonlinear curve fitting.

For the Korsmeyer-Peppas model, analysis was limited to the initial drug release phase (M_t/M_∞ = 0−60%) to evaluate early stage release kinetics.[19−22] The Peppas-Sahlin model was applied to describe the complete release profile, enabling differentiation between diffusion-controlled and relaxation-mediated transport mechanisms.[22,23]

3. RESULTS AND DISCUSSION

3.1. Basic Characterization of Individual Carriers. To evaluate the suitability of the individual carriers for drug delivery, their structural and compositional properties were analyzed. These fundamental characterizations offer insight into how each carrier interacts with timolol maleate, and how these interactions influence drug release behavior—topics further explored in the thermodynamic analysis (Section 3.2).

3.1.1. pNIPAM Nanogels Characterization. The successful synthesis of pNIPAM nanogels was confirmed by morphological and structural analysis (Figure 1A,B), which revealed a uniform spherical shape and characteristic polymer peaks, consistent with a stable hydrogel network. These features indicate that pNIPAM nanogels provide a suitable matrix for drug encapsulation and sustained release.

https://doi.org/10.1021/acsabm.5c00425
ACS Appl. Bio Mater. XXXX, XXX, XXX−XXX

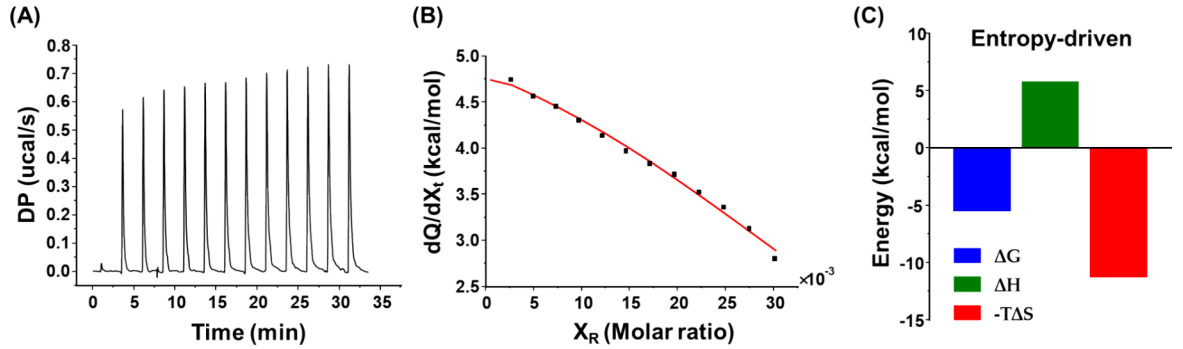

Figure 3. Isothermal titration calorimetry results of pNIPAM nanogels and timolol maleate. (A) The heat flow for each of the 18 injections, integrated heat plots (B), and the signature plots (C). Fitting the integrated data with the single binding site model the enthalpy of exchange ΔH, the binding constant K_a, and the reaction stoichiometry n are determined. It allows the calculation of the entropy ΔS and total free energy ΔG for nanocarrier-drug interaction.

Table 1. Thermodynamic Quantities of Timolol Maleate and pNIPAM Interaction Derived from ITC

carrier type	n (sites)	K_a ($\times 10^4$ M^{-1})	ΔH (kcal/mol)	ΔG (kcal/mol)	$-T\Delta S$ (kcal/mol)
pNIPAM	23.3 ± 0.47	1.05 ± 0.039	5.81 ± 0.280	−5.49	−11.3

To investigate the interaction between pNIPAM nanogels and timolol maleate, energy-dispersive X-ray spectroscopy (EDS) analysis was performed on samples incorporated into contact lenses (Figures 1C and S1). EDS signal intensity decreased progressively from the control lens (HEMA only) to lenses containing pNIPAM, and further to lenses containing both pNIPAM and timolol maleate (1200 → 700 → 400 counts), likely due to compositional changes affecting carbon (C) and oxygen (O) signal dilution or electron scattering effects. A weak nitrogen (N) signal was also detected in pNIPAM-containing samples (Figure S1), consistent with the presence of amide ($-CONH_2$) groups in polymer.

To determine whether the observed intensity reduction was due to signal dilution or actual compositional change, the C/O intensity ratio was analyzed. A gradual decrease in the ratio (2.11 → 1.96 → 1.83) was observed, indicating an increase in oxygen content relative to carbon. Since pNIPAM contains polar functional groups ($-CONH_2$), and timolol maleate introduces additional oxygen-containing moieties ($-COO^-$), the decreasing C/O ratio likely reflects the successful incorporation of timolol maleate into the pNIPAM nanogels. These findings suggest that timolol maleate is adsorbed within the nanogel network.

3.1.2. Silver Nanoparticle Characterization. Silver nanoparticles (AgNPs) exhibited well-defined, spherical morphologies, as confirmed by scanning electron microscopy (SEM) imaging (Figure 2A). Notably, SEM images of AgNPs incubated with timolol maleate showed clear nanoparticle aggregation, suggesting that timolol maleate binds to the surface of multiple AgNPs and induces interparticle bridging, thereby promoting cluster formation.

To further elucidate the underlying mechanism of this aggregation, UV−visible spectroscopy was employed to monitor the interaction between AgNPs and timolol maleate over time and under varying temperature conditions. UV−vis spectroscopy provides a sensitive measure of changes in the optical properties of AgNPs, particularly surface plasmon resonance (SPR), which is influenced by surface-binding events.

At 25 °C, spectra were recorded over an 8-h incubation period using a 1:4 molar ratio of AgNPs to timolol maleate (Figure 2B). Initially, AgNPs exhibited a distinct SPR peak at 400 nm. Over time, the peak gradually decreased in intensity, accompanied by broadening of the absorbance profile and the emergence of a shoulder extending toward 450 nm. This spectral broadening indicates progressive surface binding of timolol maleate to the AgNPs, altering the local dielectric environment and redistributing the plasmon resonance.

Since molecular interactions can be modulated by temperature, we further examined binding behavior at 25 and 40 °C (Figure S2). The AgNPs−timolol mixture incubated at 25 °C retained the SPR peak centered at 400 nm, with only minor spectral broadening up to 550 nm and negligible color change. In contrast, incubation at 40 °C resulted in a less pronounced SPR peak and substantial spectral broadening, extending across the 400−600 nm range. This was accompanied by a noticeable color shift from yellow to orange. These observations suggest enhanced drug adsorption at elevated temperatures, likely driven by increased molecular mobility and stronger surface interactions.[24]

3.2. Analysis of Drug-carrier Interactions. The preceding characterization studies (Sections 3.1.1 and 3.1.2) provided initial evidence that timolol maleate interacts with both pNIPAM nanogels, and AgNPs, as indicated by changes in elemental composition (EDS) and optical properties (UV−vis), respectively. While these results qualitatively suggest drug-carrier association, further investigation is required to understand the thermodynamic nature and structural consequences of these interactions.

To this end, we employed isothermal titration calorimetry (ITC) and differential scanning calorimetry (DSC) to quantitatively evaluate binding affinity, enthalpic and entropic contributions, and potential structural modifications following drug incorporation. These analyses offer deeper insights into the binding mechanisms of timolol maleate with each carrier, highlighting fundamental differences in interaction strength and temperature responsiveness.

3.2.1. Thermodynamic Characterization of Drug-carrier Binding. Isothermal titration calorimetry (ITC) revealed distinct thermodynamic profiles for each carrier system. For pNIPAM nanogels, the interaction with timolol maleate was characterized as an endothermic process, as indicated by

https://doi.org/10.1021/acsabm.5c00425
ACS Appl. Bio Mater. XXXX, XXX, XXX−XXX

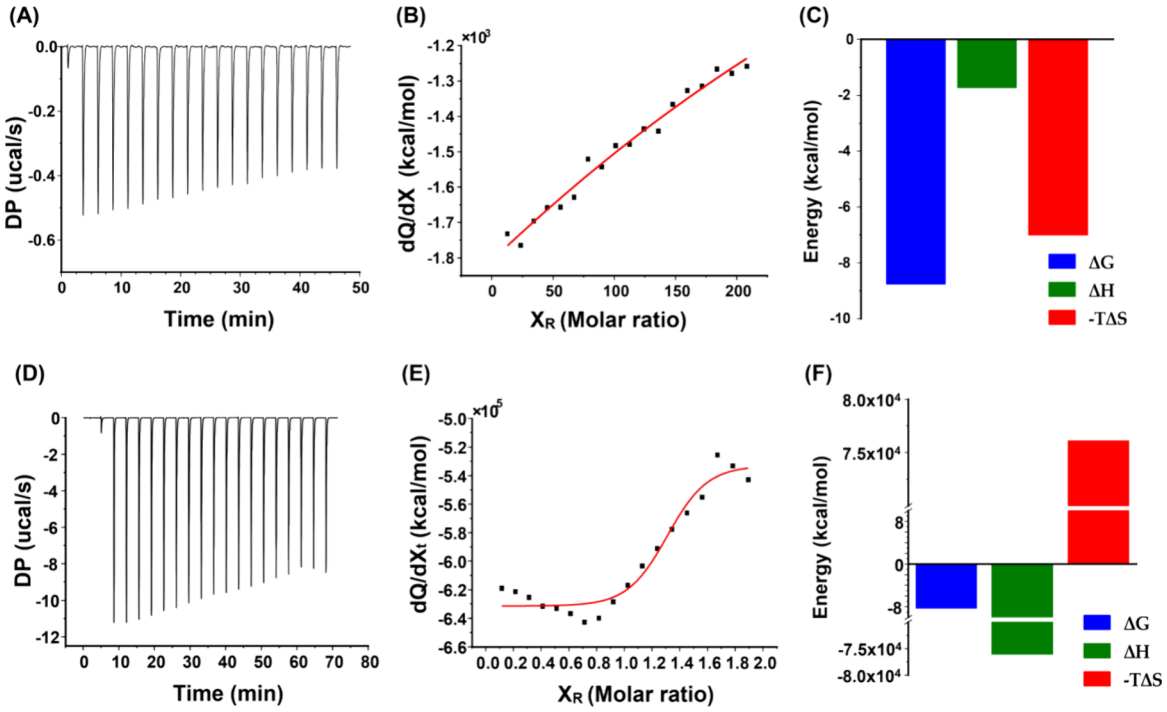

Figure 4. Isothermal titration calorimetry results of silver nanoparticle and timolol maleate (A–C) in 25 °C, (D–F) in 40 °C.

Table 2. Thermodynamic Quantities of Timolol Maleate and AgNPs Interaction Derived from ITC

carrier type	n (sites)	K_a ($\times 10^4$ M^{-1})	ΔH (kcal/mol)	ΔG (kcal/mol)	$-T\Delta S$ (kcal/mol)
AgNPs (25 °C)	0.288	265 ± 0.305	−1.75	−8.77	−7.01
AgNPs (40 °C)	1.310	68.0 ± 0.575	−7.610 ($\times 10^4$)	−8.353	7.609 ($\times 10^4$)

increases in both enthalpy and entropy (Figure 3, Table 1). This behavior is primarily attributed to the disruption of clathrate-like water structures surrounding the hydrophobic regions of both the polymer and the drug, which requires energy input to break hydrogen bonds.[25] Concurrently, the formation of hydrophobic associations between the nanogels and the drug contributes to an entropy-driven binding mechanism.

Despite the spontaneous nature of this interaction, the relatively low association constant (K_a) and the binding curve in Figure 3B suggest a weak and transient interaction.[26] The absence of an inflection point in the fitted curve further suggests this interpretation, indicating that the complex dissociates readily before equilibrium is fully reached—consistent with Ka value typically observed for hydrophobic interactions.[27,28] These findings support the conclusion that the binding is primarily driven by hydrophobic forces, which are noncovalent and typically involve minimal structural reorganization or permanent bonding.

In contrast to the entropy-driven, hydrophobic interactions observed in the pNIPAM system, binding to AgNPs appears to be predominantly enthalpy-driven, stabilized by hydrogen bonding and electrostatic interactions (Figure 4A–C, Table 2). The small negative enthalpy change ($\Delta H < 0$) and favorable free energy change ($\Delta G < 0$) indicate thermodynamically favorable binding. The high association constant ($K_a = 26.5 \times 10^5$ M^{-1}) suggests that the binding is stabilized through a combination of multiple simultaneous interactions.[26] The negative entropy contribution ($-T\Delta S < 0$) reflects increased ordering in the system, likely due to the structuring of water molecules around the nanoparticle surface.[29] This pattern of thermodynamic parameters—small exothermic ΔH, negative $-T\Delta S$, and high K_a—suggests that the interaction occurs predominantly through surface adsorption, where drug molecules bind to pre-existing sites on the AgNPs surface without inducing significant conformational or structural changes. While ITC does not directly probe structural changes of nanoparticles, the absence of a large enthalpic contribution or entropy gain typically associated with deep intercalation or structural rearrangement may indirectly support the notion that no significant alteration of the nanoparticle surface occurs during the interaction.

When the temperature was increased to 40 °C, the system exhibited a pronounced shift in thermodynamic behavior. The enthalpy change became substantially more exothermic ($\Delta H \ll 0$), suggesting enhanced interactions at specific binding sites or conformational changes at the nanoparticle interface (Figure 4D–F, Table 2). Simultaneously, the entropy contribution reversed ($-T\Delta S > 0$), indicating increased molecular disorder, possibly due to solvent reorganization. Although the binding remained spontaneous ($\Delta G < 0$), the association constant decreased ($K_a = 6.8 \times 10^5$ M^{-1}), reflecting a lower overall binding affinity at elevated temperatures. These results imply that higher temperature induces structural or interfacial changes in the system, resulting in a binding mechanism distinct from that observed under ambient conditions.

Taken together, the results indicate that pNIPAM nanogels bind timolol maleate through weak, diffusion-driven hydrophobic interactions without inducing structural alteration. In contrast, AgNPs exhibit a thermodynamically distinct binding

https://doi.org/10.1021/acsabm.5c00425
ACS Appl. Bio Mater. XXXX, XXX, XXX−XXX

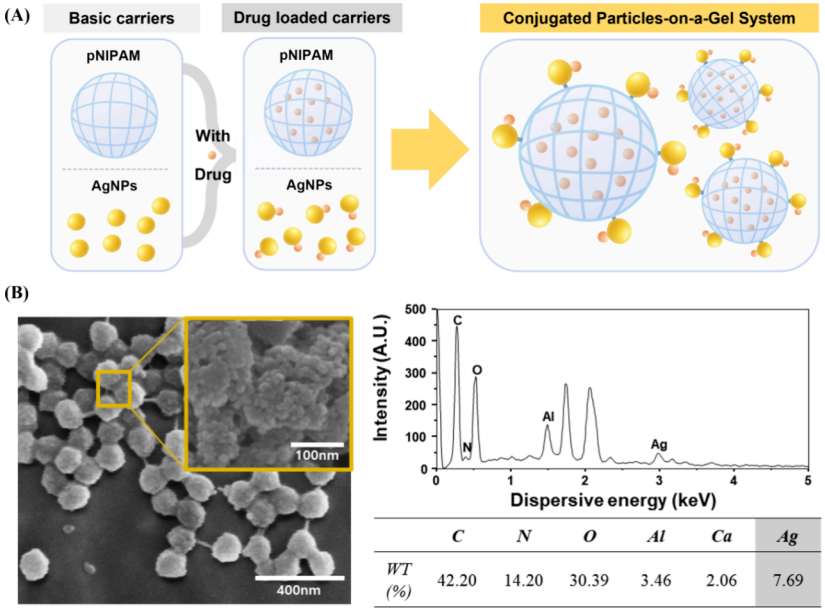

Figure 5. Design, modification, and morphological characterization of the PoG system. (A) Schematic representation of the design and modification process of the PoG system. (B) Morphological analysis of the PoG system: Cryo-SEM and EDS analysis confirming the conjugation of AgNPs onto the pNIPAM nanogels.

mode, with temperature-dependent behavior suggesting surface-specific adsorption mechanisms that remain structurally passive at lower temperatures but shift toward more dynamic or cooperative interactions under thermal stimulation.

While these thermodynamic insights offer a valuable understanding of carrier-specific drug binding, isothermal titration calorimetry (ITC) has inherent limitations. Unlike techniques such as surface plasmon resonance (SPR) or nuclear magnetic resonance (NMR) spectroscopy, which can provide spatial or kinetic resolution of binding events, ITC measures bulk heat changes across the entire system. As a result, localized, sequential, or heterogeneous interactions may be obscured. Additional analytical approaches are therefore needed to more fully characterize the complexity of drug–carrier interactions.

3.2.2. Temperature-Dependent Drug-Carrier Interaction. Differential scanning calorimetry (DSC) was employed to evaluate structural changes induced by drug incorporation, providing the complementary insight into the thermodynamic profiles obtained from ITC (Figure S3). All DSC measurements were conducted on drug carrier-loaded contact lens formulations, as the solid-state form was required for thermal analysis. This approach allowed for the detection of potential phase transitions or structural rearrangements within the carrier matrix.

DSC measurements revealed clear differences in the thermal transitions of silver nanoparticle (AgNPs) with and without timolol, indicating that drug binding induces structural changes.[30,31] These observations are consistent with the ITC findings and confirm that timolol-AgNPs interactions lead to measurable alterations in nanoparticle structure. In contrast, DSC analysis of poly(*N*-isopropylacrylamide) (pNIPAM) nanogels with and without timolol showed no significant differences in heat flow profiles. This suggests that timolol binding does not induce structural changes in the nanogel matrix, further supporting the ITC results, which indicated that pNIPAM-timolol interactions are predominantly noncovalent and diffusion-driven.

These results reinforce the conclusion that AgNPs undergo structural reorganization upon drug binding, while pNIPAM nanogels maintain their structural integrity, interacting with timolol maleate via weak, noncovalent mechanisms.

3.3. Morphology Analysis of the Particles-on-a-Gel (PoG) System. Comprehensive characterization of pNIPAM nanogels and AgNPs confirmed their successful synthesis and distinct modes of interaction with timolol maleate. These differences in binding affinity form the basis for a complementary dual-phase drug release strategy: pNIPAM nanogels support an initial diffusion-driven release, while AgNPs facilitate a more prolonged release phase. Specifically, AgNPs interact with timolol maleate in a manner that may influence diffusion by modulating the extent and rate of bond dissociation. The most plausible mechanism involves sulfide bonding between a thiol group of timolol and the silver surfaces.[32−34]

In contrast, pNIPAM interacts with timolol maleate via hydrophobic forces, such that drug diffusion is primarily driven by the concentration gradient within the nanogel. A higher concentration of loosely bound drug molecules near the surface can accelerate the initial diffusion rate, highlighting the importance of managing surface-bound drug levels to maintain a consistent release profile.

Building on these insights, we developed a particles-on-a-gel (PoG) system to regulate diffusion and extend drug release duration. Structural analysis using SEM and EDS confirmed the successful integration of AgNPs with the pNIPAM nanogels, forming a raspberry-like morphology (Figure 5B). This unique structural configuration effectively combines the advantages of both carriers, further optimizing drug release kinetics.

3.4. Drug Release Profile of Particles-on-a-Gel System. The drug release characteristics of the PoG system were evaluated by incorporating the formulation into contact lenses and monitoring its release profile over time. To contextualize the release data, we first quantified the amount of drug associated with each carrier prior to lens fabrication.

https://doi.org/10.1021/acsabm.5c00425
ACS Appl. Bio Mater. XXXX, XXX, XXX−XXX

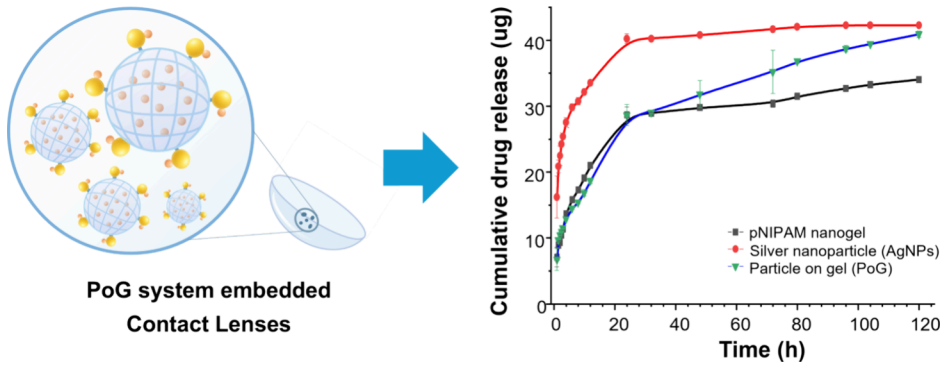

Figure 6. Comparative analysis of cumulative drug release from three different carriers.

This was achieved by measuring UV−vis absorbance after centrifugation to separate bound drug. The corresponding drug-loading capacities were presented in Figure S4A. These results provide a reference point for interpreting the subsequent release profiles.

Comparative release patterns for the PoG system and its individual components are presented in Figure 6. Among the carriers, the silver nanoparticles (AgNPs) system exhibited the highest cumulative drug release (42.25 μg), while the pNIPAM nanogels system released the lowest amount (34.02 μg). The PoG system demonstrated a total release comparable to that of AgNPs.

Within the first 24 h, AgNPs showed the most rapid release rate, while both pNIPAM and PoG systems displayed similar, slower release kinetics. After 24 h, the drug release from AgNPs declined sharply, whereas the pNIPAM system continued to release small amounts gradually. Notably, the PoG system maintained a steady and sustained release profile beyond the initial period.

We initially hypothesized that drug release from pNIPAM nanogels would be governed by a concentration gradient due to their noncovalent, diffusion-driven interactions, while AgNPs, which form stronger chemical bonds, would provide a slower release. Contrary to this expectation, AgNPs exhibited a remarkably rapid initial release. This unexpected behavior is likely attributable to the oxidative instability of AgNPs; once oxidized, even strongly bound timolol maleate may dissociate rapidly due to degradation of the nanoparticle structure.

In contrast, the PoG system demonstrated the anticipated prolonged release effect (Scheme 1). The incorporation of pNIPAM nanogels likely contributed to this sustained release by mitigating AgNPs oxidation.[35−37] To investigate this stabilization effect, we monitored changes in the color of AgNPs over 24-h period (Figure S5). AgNPs alone exhibited complete discoloration, consistent with full oxidation and conversion to silver ions.[38−40] In comparison, AgNPs embedded within the PoG system exhibited a visible color shift but did not become fully transparent, suggesting that the pNIPAM nanogels provide partial protection against oxidative degradation.

Additionally, the PoG system appeared to reduce the number of loosely bound drug molecules on the surface of the pNIPAM nanogels. Although we initially expected this reduction to markedly suppress early phase diffusion, only a minor change was observed. However, given that the total amount of drug released increased while the initial burst release was reduced, it is likely that fewer surface-bound drug molecules were prematurely lost, resulting in a more sustained and controlled release profile. While this suggests enhanced temporal control of drug delivery, it does not necessarily indicate higher release efficiency relative to the initial loading. Only 67% of the drug loaded in the PoG system was released, compared to 75 and 78% in the pNIPAM and AgNP systems, respectively (Figure S4B). This difference may reflect stronger drug retention, restricted diffusion, or structural entrapment within the PoG matrix.

Scheme 1. Mechanism Enabling Prolonged Drug Release in the PoG System

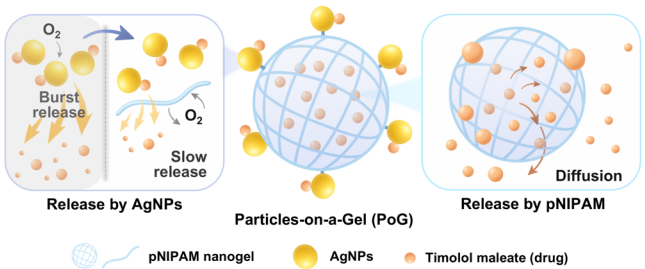

3.5. Interpretation of Drug Release Mechanisms of Particles-on-a-Gel System. To further elucidate the mechanisms governing drug release from the PoG system, kinetic modeling was employed to quantify the relative contributions of diffusion and carrier relaxation. The Korsmeyer-Peppas model was applied to analyze the initial release phase up to 60% drug release.[19−22] In this model, the release exponent (n) provides insight into the dominant transport mechanism: $n \leq 0.45$ indicates Fickian diffusion, $0.45 < n < 0.89$ suggests anomalous (non-Fickian) transport, and $n \geq 0.89$ corresponds to case-II transport, typically associated with polymer relaxation.[41,42] The n values for all three systems fall within the Fickian diffusion range, indicating that the early stage release is primarily diffusion-controlled for each carrier (Table 3).

Table 3. Kinetic Values of Three Types of Nanocarrier Based on Kormeyer-Peppas Model

	Korsmeyer−Peppas kinetic profile			
type	KP	n	R^2	drug release mechanism
pNIPAM	21.170	0.429	0.9644	quasi-Fickian
AgNPs	40.391	0.378	0.9668	quasi-Fickian
PoG	22.361	0.337	0.9972	quasi-Fickian

https://doi.org/10.1021/acsabm.5c00425
ACS Appl. Bio Mater. XXXX, XXX, XXX−XXX

Since the Korsmeyer-Peppas model primarily describes the initial release behavior, the Peppas-Sahlin model was also used to distinguish the contributions of diffusion and carrier relaxation throughout the entire release process.[22,23] The diffusion-related parameter k_1 was highest for AgNPs, followed by pNIPAM and PoG, confirming diffusion as the dominant release mechanism across all systems (Table 4). However, the carrier relaxation constant k_2 was negative for both pNIPAM and AgNPs, indicating negligible contributions from carrier relaxation.[43] In contrast, the PoG system exhibited a positive k_2 value, suggesting that polymer relaxation plays a secondary but meaningful role in modulating drug release. These mechanistic differences were further supported by the transport exponent (m) values, also summarized in Table 4.

Table 4. Kinetic Values of Three Types of Nanocarrier Based on Peppas-Sahlin Model

	Peppasr−Sahlin kinetic profile				
type	k_1	k_2	m	R^2	drug release mechanism
pNIPAM	26.111	−1.761	0.436	0.9880	anomalous transport
AgNPs	57.335	−8.208	0.279	0.9937	quasi-Fickian
PoG	21.368	5.569	0.209	0.9975	quasi-Fickian

These kinetic findings provide a quantitative framework for interpreting the thermodynamic observations. The unexpectedly rapid release from AgNPs, despite their strong chemical affinity for timolol maleate, is reflected in the kinetic model as a diffusion-dominated process. Carrier relaxation in the Peppas-Sahlin model typically characterizes polymeric systems where swelling, matrix relaxation, or structural rearrangements governs drug release. Since AgNPs are inorganic and undergo oxidative degradation rather than gradual structural transformation, their release behavior does not contribute to a positive k_2, reinforcing their classification as diffusion-driven.

For the pNIPAM nanogels, the detection of anomalous transport—rather than purely Fickian diffusion—likely reflects nanogel swelling effects. However, the negative k_2 value indicates that polymer relaxation is not a major contributor to the release process.

Unlike single carrier systems, where release is primarily governed by either diffusion or carrier relaxation, the PoG system exhibits a synergistic mechanism that integrates both effects. While diffusion remains the primary release driver, the emergence of a positive k_2 value suggests that pNIPAM's stabilization of AgNPs modifies the drug release pathway. This observation aligns with thermodynamic data, which showed that pNIPAM nanogels mitigate AgNPs oxidation, contributing to prolonged drug retention. The kinetic model further supports this, as the presence of a relaxation component ($k_2 > 0$) in the PoG system implies that nanogel-mediated stabilization affects not only the extent of AgNPs oxidation but also the temporal dynamics of drug diffusion.

Together, these findings highlight the importance of integrating kinetic and thermodynamic analyses to fully understand drug release behavior, offering a design rationale for developing advanced nanocarrier systems with enhanced release control.

3.6. Potential of the Particles-on-a-Gel System for Sustained Glaucoma Treatment. *3.6.1. Suitability of the Release Profiles.* Given the focus on glaucoma therapy, it is essential to assess whether the PoG system provides a release profile appropriate for sustained intraocular pressure (IOP) control. To evaluate this, we analyzed both the drug release kinetics and therapeutic relevance using established clinical benchmarks.

Effective glaucoma management requires maintaining drug concentrations above the therapeutic threshold. However, conventional eye drops are highly inefficient, with only about 5% of the administered dose reaching ocular tissues. For instance, a 50 μL drop of a 0.5% timolol maleate solution delivers approximately 12.5 μg of drug systemically. To address this limitation, we adopted a contact lens-based drug delivery platform, leveraging its prolonged corneal contact time and enhanced drug retention to improve ocular bioavailability. Based on reported absorption efficiencies of up to 50% with contact lenses, we set a target drug release of 25 μg within the first 24 h to achieve therapeutic exposure comparable to once-daily eye drop administration.[44]

While achieving therapeutic levels within the first 24 h is essential for initiating IOP reduction, maintaining a residual drug presence beyond this period is also important for attenuating pressure rebound. Timolol maleate exhibits a characteristic pharmacodynamic profile when delivered via sustained-release system: IOP is maximally reduced within the first 24 h, followed by a gradual return to baseline over

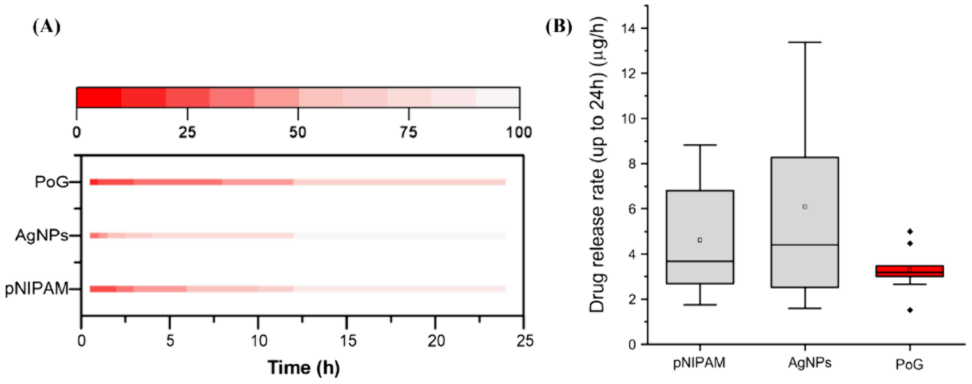

Figure 7. Drug release profiles of three different carriers within 24 h; (A) cumulative drug release percentage, normalized to 100%. The color scale has been adjusted such that red indicates a lower percentage of total release (approaching 0%), while white represents a higher percentage (approaching 100%), with 50% as the transition point. (B) Box plot analysis of drug release rates. The data was calculated based on the kinetic drug release data. ☐ 25% ~ 75%, I Range within 1.5IQR, ___ Median Line, ☐ Mean, ◆ Outliers.

https://doi.org/10.1021/acsabm.5c00425
ACS Appl. Bio Mater. XXXX, XXX, XXX−XXX

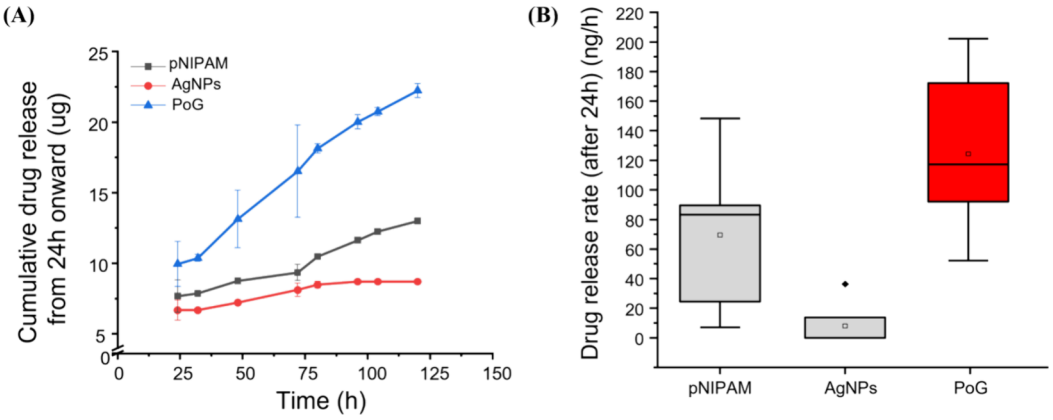

Figure 8. Drug release profiles of three different carriers beyond 24 h; (A) cumulative drug release percentage after 24 h. (B) Box plot analysis of drug release rates beyond 24 h.

approximately 120 h.[45−47] Although drug concentrations in tear film may remain detectable for up to 56 h, this alone is insufficient to sustain maximal therapeutic effect.[45] However, continued drug availability during the postpeak period can help moderate the rate of IOP increase, thus reducing short-term fluctuations that are known to exacerbate glaucoma progression. Based on this rationale, we defined 120 h as the target duration for extended release.

Having defined the desired release window, we next examined whether the PoG system could deliver timolol maleate in a controlled and sustained manner consistent with this therapeutic goal. As shown in Figure 6, all tested systems released more than 25 μg within the first 24 h, meeting the minimum requirement for initial IOP reduction. To assess release consistency beyond the initial dose, we analyzed the temporal drug release patterns in detail. Figure 7A illustrates the release dynamics: both AgNPs and pNIPAM nanogels exhibited initial burst release profiles, whereas the PoG system maintained a more gradual and sustained drug release. This behavior is crucial for ensuring stable drug availability in the ocular environment over an extended period.

Figure 7B further supports this finding by visualizing release rate variability using box plot. The PoG system exhibited the narrowest interquartile range (25−75%), indicating the most consistent release profile among the tested systems. Such uniformity is a key feature of effective sustained-release systems, as it helps minimize fluctuations in drug concentration and supports consistent therapeutic efficacy.

Together, these results demonstrate that the PoG system fulfills the therapeutic requirements for both immediate and prolonged IOP control, maintaining drug release for up to 120 h (Figure 8).

3.6.2. Practical Considerations for Contact Lens-Based Drug Delivery. In addition to sustained drug release, practical factors that affect usability and patient comfort must also be considered for clinical translation—particularly in contact lens—based systems, where any compromise in lens transparency can directly impair vision and reduce compliance. As shown in Figure S6, contact lenses incorporating individual carrier systems exhibited a noticeable loss in light transmittance, with postrelease values dropping by more than 20%. In contrast, lenses loaded with the PoG system retained over 70% transmittance after drug release, indicating minimal visual interference. These findings highlight the PoG system's suitability for long-term ocular drug delivery, as it maintains both functional drug release and optical clarity—two essential prerequisites for successful clinical translation.

4. CONCLUSION

This study presents a "Particles-on-a-Gel" (PoG) system that regulates drug release by leveraging differential nanocarrier affinities. By integrating poly(*N*-isopropylacrylamide) (pNIPAM) nanogels and silver nanoparticles (AgNPs), the PoG system achieves controlled and sustained drug delivery of timolol maleate, effectively balancing the initial burst phase with prolonged release.

Thermodynamic and kinetic analyses revealed distinct drug-carrier interaction mechanisms that govern release behavior. The pNIPAM nanogels facilitated diffusion-driven release via hydrophobic interactions, while AgNPs enabled stronger drug retention through surface-based interactions. By combining these carriers, the PoG system achieves a tunable and extended release profile, made possible not simply by additive effects, but by the interplay of complementary binding behaviors.

The PoG system also demonstrated structural integrity and maintained lens transparency after drug release, highlighting its feasibility for contact lens-based ocular drug delivery. Compared to single-carrier systems, the PoG platform offers improved control over release kinetics and better preserves optical clarity—both critical factors for patient compliance and long-term therapeutic effectiveness.

Beyond ophthalmic applications, this dual-carrier approach offers a generalizable framework for nanocarrier-based drug delivery in chronic disease management. Future work should focus on in vivo evaluation, long-term safety studies, and further optimization to support clinical translation. By bridging fundamental drug-carrier interaction insights with practical design considerations, this study contributes to the advancement of next-generation sustained-release systems for clinical therapeutic use.

■ ASSOCIATED CONTENT

Supporting Information

The Supporting Information is available free of charge at https://pubs.acs.org/doi/10.1021/acsabm.5c00425.

SEM and EDS analysis of samples with and without pNIPAM and timolol maleate (Figure S1); temperature-dependent drug adsorption onto nanoparticle surfaces, examined at 25 and 40 °C (Figure S2); differential scanning calorimetry (DSC) profiles of nanocarrier-

https://doi.org/10.1021/acsabm.5c00425
ACS Appl. Bio Mater. XXXX, XXX, XXX−XXX

drug-contact lens systems (Figure S3); pNIPAM nanogels in stabilizing AgNPs; time-dependent color changes of silver nanoparticles over 24 h; characterization of the PoG system and evaluation of the oxidative stability of silver nanoparticles (Figure S4); and changes in optical transmittance of lenses containing nanocarriers before and after release (Figure S5) (PDF)

AUTHOR INFORMATION

Corresponding Author

Hyeran Noh − *Department of Optometry, Seoul National University of Science and Technology, Seoul 01811, Korea; SeoulTech-KIRAMS Graduate School of Biomedical Science and Engineering, Seoul National University of Science and Technology, Seoul 01811, South Korea;* orcid.org/0000-0003-4667-6754; Email: hrnoh@seoultech.ac.kr

Authors

Hyeonah Lee − *Department of Optometry, Seoul National University of Science and Technology, Seoul 01811, Korea*

Serim Byun − *Department of Optometry, Seoul National University of Science and Technology, Seoul 01811, Korea*

Moonyoung Kim − *Department of Optometry, Seoul National University of Science and Technology, Seoul 01811, Korea*

Hyeokjung Kim − *Department of Optometry, Seoul National University of Science and Technology, Seoul 01811, Korea;* orcid.org/0000-0002-4205-1397

Complete contact information is available at: https://pubs.acs.org/10.1021/acsabm.5c00425

Author Contributions

The manuscript was written through contributions of all authors. All authors have given approval to the final version of the manuscript. H.L. and S.B. contributed equally.

Notes

The authors declare no competing financial interest.

ACKNOWLEDGMENTS

This work was supported by the Seoul National University of Science and Technology.

REFERENCES

(1) Jiang, Y.-Q.; Chen, J.-P.; Dong, Y.-J.; Zhou, F.-J.; Tian, C.-W.; Chen, C.-Q. Delivery System for Targeted Drug Therapy in Chronic Diseases. *J. Explor. Res. Pharmacol.* **2022**, *7* (2), 112−122.

(2) Yanar, F.; Carugo, D.; Zhang, X. Hybrid Nanoplatforms Comprising Organic Nanocompartments Encapsulating Inorganic Nanoparticles for Enhanced Drug Delivery and Bioimaging Applications. *Molecules* **2023**, *28* (15), 5694.

(3) Weng, Y.-H.; Ma, X.-W.; Che, J.; Li, C.; Liu, J.; Chen, S.-Z.; Wang, Y.-Q.; Gan, Y.-L.; Chen, H.; Hu, Z.-B.; Nan, K.-H.; Liang, X.-J. Nanomicelle-Assisted Targeted Ocular Delivery with Enhanced Antiinflammatory Efficacy In Vivo. *Adv. Sci.* **2018**, *5* (1), No. 1700455.

(4) Singh, A. P.; Biswas, A.; Shukla, A.; Maiti, P. Targeted Therapy in Chronic Diseases Using Nanomaterial-Based Drug Delivery Vehicles. *Signal Transduct. Target. Ther.* **2019**, *4* (1), 33.

(5) Lombardo, D.; Kiselev, M. A.; Caccamo, M. T. Smart Nanoparticles for Drug Delivery Application: Development of Versatile Nanocarrier Platforms in Biotechnology and Nanomedicine. *J. Nanomater.* **2019**, *2019*, No. 3702518.

(6) Rad, M. E.; Soylukan, C.; Kulabhusan, P. K.; Günaydın, B. N.; Yüce, M. Material and Design Toolkit for Drug Delivery: State of the Art, Trends, and Challenges. *ACS Appl. Mater. Interfaces* **2023**, *15* (48), 55201−55231.

(7) Salahpour Anarjan, F. Active Targeting Drug Delivery Nanocarriers: Ligands. *Nano-Struct. & Nano-Objects* **2019**, *19*, No. 100370.

(8) Bertrand, N.; Wu, J.; Xu, X.; Kamaly, N.; Farokhzad, O. C. Cancer Nanotechnology: The Impact of Passive and Active Targeting in the Era of Modern Cancer Biology. *Adv. Drug Delivery Rev.* **2014**, *66*, 2−25.

(9) Lee, K.; Kim, T.; Kim, Y. M.; Yang, K.; Choi, I.; Roh, Y. H. Multifunctional DNA Nanogels for Aptamer-Based Targeted Delivery and Stimuli-Triggered Release of Cancer Therapeutics. *Macromol. Rapid Commun.* **2021**, *42* (2), No. 2000457.

(10) Bargeron, B. C.; Farrell, R. A.; Green, W. R.; McCally, R. L. Corneal Damage from Exposure to Ir Radiation. *Health Phys.* **1981**, *40* (6), 855−862.

(11) Ham, W. T.; Mueller, H. A.; Sliney, D. H. Retinal Sensitivity to Damage from Short Wavelength Light. *Nature* **1976**, *260* (5547), 153−155.

(12) Trucillo, P. Drug Carriers: A Review on the Most Used Mathematical Models for Drug Release. *Processes* **2022**, *10* (6), 1094.

(13) Gao, Y.; Shi, Y.; Wang, L.; Kong, S.; Du, J.; Lin, G.; Feng, Y. Advances in Mathematical Models of the Active Targeting of Tumor Cells by Functional Nanoparticles. *Comput. Methods Programs Biomed.* **2020**, *184*, No. 105106.

(14) Laracuente, M.-L.; Yu, M. H.; McHugh, K. J. Zero-Order Drug Delivery: State of the Art and Future Prospects. *J. Controlled Release* **2020**, *327*, 834−856.

(15) ElShaer, A.; Mustafa, S.; Kasar, M.; Thapa, S.; Ghatora, B.; Alany, R. Nanoparticle-Laden Contact Lens for Controlled Ocular Delivery of Prednisolone: Formulation Optimization Using Statistical Experimental Design. *Pharmaceutics* **2016**, *8* (2), 14.

(16) Nasr, F. H.; Khoee, S.; Dehghan, M. M.; Chaleshtori, S. S.; Shafiee, A. Preparation and Evaluation of Contact Lenses Embedded with Polycaprolactone-Based Nanoparticles for Ocular Drug Delivery. *Biomacromolecules* **2016**, *17* (2), 485−495.

(17) Rodrigues, F. S. C.; Campos, A.; Martins, J.; Ambrósio, A. F.; Campos, E. J. Emerging Trends in Nanomedicine for Improving Ocular Drug Delivery: Light-Responsive Nanoparticles, Mesoporous Silica Nanoparticles, and Contact Lenses. *ACS Biomater. Sci. Eng.* **2020**, *6* (12), 6587−6597.

(18) Fiévet, F.; Ammar-Merah, S.; Brayner, R.; Chau, F.; Giraud, M.; Mammeri, F.; Peron, J.; Piquemal, J.-Y.; Sicard, L.; Viau, G. The Polyol Process: A Unique Method for Easy Access to Metal Nanoparticles with Tailored Sizes, Shapes and Compositions. *Chem. Soc. Rev.* **2018**, *47* (14), 5187−5233.

(19) Korsmeyer, R. W.; Gurny, R.; Doelker, E.; Buri, P.; Peppas, N. A. Mechanisms of Solute Release from Porous Hydrophilic Polymers. *Int. J. Pharm.* **1983**, *15* (1), 25−35.

(20) Zhu, W.; Long, J.; Shi, M. Release Kinetics Model Fitting of Drugs with Different Structures from Viscose Fabric. *Materials* **2023**, *16* (8), 3282.

(21) Heredia, N. S.; Vizuete, K.; Flores-Calero, M.; Pazmiño V, K.; Pilaquinga, F.; Kumar, B.; Debut, A.; Annamalai, P. K. Comparative Statistical Analysis of the Release Kinetics Models for Nanoprecipitated Drug Delivery Systems Based on Poly(Lactic-Co-Glycolic Acid). *PLoS One* **2022**, *17* (3), No. e0264825.

(22) Talevi, A.; Ruiz, M. E. Korsmeyer-Peppas, Peppas-Sahlin, and Brazel-Peppas: Models of Drug Release. In: *The ADME Encyclopedia*; Springer: Cham, 2021; 1−9.

(23) Ritger, P. L.; Peppas, N. A. A Simple Equation for Description of Solute Release I. Fickian and Non-Fickian Release from Non-Swellable Devices in the Form of Slabs, Spheres, Cylinders or Discs. *J. Controlled Release* **1987**, *5* (1), 23−36.

(24) Klingler, A.; Wetzel, B.; Krüger, J.-K. Temperature-Controlled Molecular Bonding Hysteresis: Interphase Dynamics of a Nanoparticle-Modified Polymer Network. *J. Phys. Chem. Lett.* **2024**, *15* (13), 3576−3580.

(25) Sun, Q. The Hydrophobic Effects: Our Current Understanding. *Molecules* **2022**, *27* (20), 7009.

(26) Amponsah-Efah, K. K.; Mistry, P.; Eisenhart, R.; Suryanarayanan, R. The Influence of the Strength of Drug−Polymer Interactions on the Dissolution of Amorphous Solid Dispersions. *Mol. Pharmaceutics* **2021**, *18* (1), 174−186.
(27) Ciulli, A. Biophysical Screening for the Discovery of Small-Molecule Ligands. *Methods Mol. Biol.* **2013**, *1008*, 357−388.
(28) Kirley, T. L.; Norman, A. B. Isothermal Titration Calorimetry Determination of Thermodynamics of Binding of Cocaine and Its Metabolites to Humanized H2E2 Anti-Cocaine MAb. *Biochem. Biophys. Rep.* **2022**, *32*, No. 101354.
(29) Li, J.; Hou, C.; Ma, X.; Guo, S.; Zhang, H.; Shi, L.; Liao, C.; Zheng, B.; Ye, L.; Yang, L.; He, X. Entropy-Enthalpy Compensations Fold Proteins in Precise Ways. *Int. J. Mol. Sci.* **2021**, *22* (17), 9653.
(30) Maule, I.; Razzetti, G.; Restelli, A.; Palmieri, A.; Colombo, C.; Ballini, R. Thermal Stability Evaluation of Nitroalkanes with Differential Scanning Calorimetry. *Org. Process Res. Dev.* **2021**, *25* (4), 781−788.
(31) Khan, M. F.; Rahman, M. M.; Xin, Y.; Mustafa, A.; Smith, B. J.; Ottemann, K. M.; Roujeinikova, A. Determination of Protein−Ligand Binding Affinities by Thermal Shift Assay. *ACS Pharmacol. Transl. Sci.* **2024**, *7* (10), 3096−3107.
(32) Bayram, S.; Zahr, O. K.; Blum, A. S. Short Ligands Offer Long-Term Water Stability and Plasmon Tunability for Silver Nanoparticles. *RSC Adv.* **2015**, *5* (9), 6553−6559.
(33) Das, U.; Theisen, R.; Hanket, G.; Upadhyaya, A.; Rohatgi, A.; Hua, A.; Weinhardt, L.; Hauschild, D.; Heske, C. Sulfurization as a Promising Surface Passivation Approach for Both N- and p-Type Si. In *Proceedings of the 47th IEEE Photovoltaic Specialists Conference (PVSC)*; IEEE: Piscataway, NJ, 2020; 1167−1170.
(34) Salvi, A.; Bankhele, P.; Jamil, J.; Chitnis, M. K.; Njie-Mbye, Y. F.; Ohia, S. E.; Opere, C. A. Effect of Hydrogen Sulfide Donors on Intraocular Pressure in Rabbits. *J. Ocul. Pharmacol. Ther.* **2016**, *32* (6), 371−375.
(35) Biswas, S.; Kim, D.-K.; Nam, I.-W.; Choi, M.; Bae, J.-H.; Kim, H. Highly Conductive and Thermally Stable Nanoparticle-Conjugated Polymer Compounds through Environmentally Friendly in Situ Synthesis. *Prog. Org. Coat.* **2020**, *142*, No. 105606.
(36) Madkour, M.; Bumajdad, A.; Al-Sagheer, F. To What Extent Do Polymeric Stabilizers Affect Nanoparticles Characteristics? *Adv. Colloid Interface Sci.* **2019**, *270*, 38−53.
(37) Ballesteros, C. A. S.; Bernardi, J. C.; Correa, D. S.; Zucolotto, V. Controlled Release of Silver Nanoparticles Contained in Photoresponsive Nanogels. *ACS Appl. Bio. Mater.* **2019**, *2* (2), 644−653.
(38) Cunningham, B.; Engstrom, A. M.; Harper, B. J.; Harper, S. L.; Mackiewicz, M. R. Silver Nanoparticles Stable to Oxidation and Silver Ion Release Show Size-Dependent Toxicity In Vivo. *Nanomaterials* **2021**, *11* (6), 1516.
(39) Bonilla-Gameros, L.; Chevallier, P.; Copes, F.; Sarkissian, A.; Mantovani, D. The Oxidation State of Ag Nanoparticles Highly Affects the Release of Ag Ions without Compromising the Mechanical Performance and the Safety of Amorphous Hydrogenated Carbon Coatings. *Diam. Relat. Mater.* **2022**, *130*, No. 109430.
(40) Ongtanasup, T.; Kamdenlek, P.; Manaspon, C.; Eawsakul, K. Green-Synthesized Silver Nanoparticles from Zingiber Officinale Extract: Antioxidant Potential, Biocompatibility, Anti-LOX Properties, and in Silico Analysis. *BMC Complement. Med. Ther.* **2024**, *24* (1), 84.
(41) Olejnik, A.; Kapuscinska, A.; Schroeder, G.; Nowak, I. Physico-Chemical Characterization of Formulations Containing Endomorphin-2 Derivatives. *Amino Acids* **2017**, *49* (10), 1719−1731.
(42) Moodley, T.; Singh, M. Polymeric Mesoporous Silica Nanoparticles for Combination Drug Delivery In Vitro. *Biointerface Res. Appl. Chem.* **2021**, *11* (4), 11905−11919.
(43) Rentería-Urquiza, M.; Flores-Rojas, G. G.; Gómez-Lázaro, B.; López-Saucedo, F.; Vera-Graziano, R.; Mendizabal, E.; Bucio, E. Lignocellulosic Membranes Grafted with N-Vinylcaprolactam Using Radiation Chemistry: Load and Release Capacity of Vancomycin. *Polymers* **2024**, *16* (4), 551.
(44) Maulvi, F.; Soni, T. G.; Shah, D. O. Effect of Timolol Maleate Concentration on Uptake and Release from Hydrogel Contact Lenses Using Soaking Method. *J. Pharm. Appl. Sci.* **2014**, *1*, 17−23.
(45) Maulvi, F. A.; Patel, A. R.; Shetty, K. H.; Desai, D. T.; Shah, D. O.; Willcox, M. D. P. Chitosan Nanoparticles Laden Contact Lenses for Enzyme-Triggered Controlled Delivery of Timolol Maleate: A Promising Strategy for Managing Glaucoma. *Drug Delivery Transl. Res.* **2024**, *14* (11), 3212−3224.
(46) Maulvi, F. A.; Patil, R. J.; Desai, A. R.; Shukla, M. R.; Vaidya, R. J.; Ranch, K. M.; Vyas, B. A.; Shah, S. A.; Shah, D. O. Effect of Gold Nanoparticles on Timolol Uptake and Its Release Kinetics from Contact Lenses: In Vitro and in Vivo Evaluation. *Acta Biomater* **2019**, *86*, 350−362.
(47) Shokry, M.; Hathout, R. M.; Mansour, S. Exploring Gelatin Nanoparticles as Novel Nanocarriers for Timolol Maleate: Augmented in-Vivo Efficacy and Safe Histological Profile. *Int. J. Pharm.* **2018**, *545*, 229−239.

https://doi.org/10.1021/acsabm.5c00425
ACS Appl. Bio Mater. XXXX, XXX, XXX−XXX